Journal of Alloys and Compounds 488 (2009) 386–391

Contents lists available at ScienceDirect

Journal of Alloys and Compounds

journal homepage: www.elsevier.com/locate/jallcom

Nanocomposite thermite powders prepared by cryomilling

Carlo Badiola, Mirko Schoenitz, Xiaoying Zhu, Edward L. Dreizin*

New Jersey Institute of Technology, Newark, NJ 07103, USA

ARTICLE INFO

Article history:
Received 1 May 2009
Received in revised form 28 August 2009
Accepted 31 August 2009
Available online 8 September 2009

Keywords:
Metals and alloys
Nanostructured materials
Mechanical alloying
Calorimetry
X-ray diffraction
Thermal analysis

ABSTRACT

Reactive nanocomposite materials have been recently prepared by Arrested Reactive Milling (ARM), a method based on mechanical milling of component powders to form micron-sized composite particles where components are mixed on a scale of about 100 nm. The milling temperature affects both the refinement rate and the final product properties. In this paper we report an effort to prepare Al–CuO reactive nanocomposite powders at cryogenic temperatures. The material was processed in a liquid nitrogen bath using steel vials and balls of different sizes as milling media. The number and dimensions of the milling balls as well as the milling time were systematically varied. The products were characterized by X-ray diffraction, particle size analysis, and scanning electron microscopy. Thermal characteristics were studied using a custom wire-ignition setup and differential scanning calorimetry. Results show that the uniformity of mixing and reactivity of the nanocomposite powders can be improved using milling at cryogenic temperatures.

1. Introduction

Nanocomposite reactive materials, in particular, thermites, are gaining much attention after recent studies showing that high reaction rates are possible to achieve in addition to the substantial reaction enthalpy when the reactive components are mixed on the scale of about 100 nm, see, for example review [1] and Refs. [2–8]. Among different techniques used to prepare such nanocomposite materials, Arrested Reactive Milling (ARM) method offers an inexpensive and scalable technique that is very versatile and can be applied to a wide range of reactive material compositions [9–14]. The ARM-prepared powders comprise micron-sized particles, where each particle is a fully dense composite with nano-sized inclusions of one component embedded in a matrix of the second component. The powders are prepared by high-energy mechanical milling of micron-sized powders of the individual components. Both shaker and planetary mills operated at room temperature were used in previous studies to prepare reactive nanocomposite materials by ARM. The milling is interrupted (or arrested) before the highly exothermic and typically self-sustaining reaction between the material components is triggered mechanically. Previous work showed that a slight reduction in the temperature at which the reactive materials are milled results in a substantial change in the product properties [15]. In parallel, substantial efforts have been reported on mechanical alloying performed at cryogenic temperatures [16,17]. The material properties, altered at cryogenic temperatures result in better-refined structures produced during shorter milling times. In some experiments, the phase make up of the mechanically alloyed compound was observed to be different depending on the milling temperature. Cryomilling was recently used to prepare new hydrogen-storage materials with improved properties [18,19], reduce the powder size to nanoscale [20], and prepare nanocomposite materials [21].

Mechanical alloying, as ARM, relies on high-energy ball milling to refine the material structure. The key differences of ARM from mechanical alloying are that the starting components are capable of a highly exothermic reaction, and that the initiation of such a reaction is undesirable. Thus, it is expected that ARM performed at cryogenic temperatures is an attractive method of preparing materials with refined and intimately mixed reactive components for which the low processing temperature suppresses chemical interaction. This paper investigates the feasibility of preparation reactive nanocomposite materials by ARM at a cryogenic temperature.

2. Experimental

The experiments in this study were performed on a SPEX Certiprep 6815 Freezer/Mill. In this vibratory mill, four stainless steel vials are submerged in liquid nitrogen, in a horizontal orientation. The vial dimensions are 7/8 in. diameter and 3 7/8 in. length. The milling vials are closed at the ends with relatively loosely fitting end caps. The four vials are arranged in a group so that two vials are positioned above the other two. The individual vials are separated with a divider. Two solenoids impose an alternating magnetic field that moves magnetic milling media inside the vials back and forth along the vials' axes. Collisions occur among the milling media and between the media and the end caps of the milling vials. Available milling media are single cylindrical impactors and hardened steel balls with different diameters.

* Corresponding author. Tel.: +1 973 596 5751.
E-mail address: dreizin@njit.edu (E.L. Dreizin).

0925-8388/$ – see front matter © 2009 Elsevier B.V. All rights reserved.
doi:10.1016/j.jallcom.2009.08.146

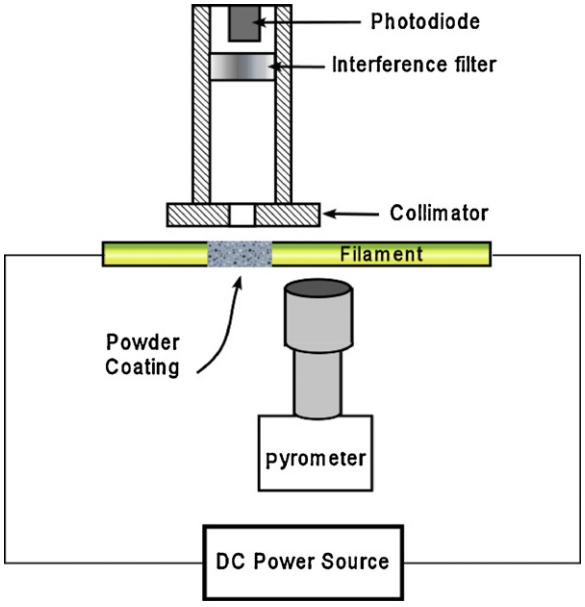

Fig. 1. Simplified diagram of the heated filament ignition setup.

Aluminum (−325 mesh, <45 μm, 99.5%, Atlantic Equipment Engineering), and CuO (25 μm, 99+%, Sigma–Aldrich) were placed in the milling vials in order to prepare nanocomposite powders with overall compositions of 12Al·3CuO. These metal-rich thermite compositions, which are substantially less reactive than stoichiometric compositions, were selected for initial cryogenic milling experiments in order to minimize possible damage to the equipment in case of undesirable thermite reaction occurring during the milling. Milling vials were loaded at room temperature in ambient air. The end caps do not seal hermetically; therefore, loading in a protective atmosphere was not attempted. After loading, the vials were pre-cooled by immersing in liquid nitrogen.

Milling parameters varied in experiments were the milling time (30–1200 min), the mass, and number of the milling media (various combinations of 7/16 in. and 3/16 in. steel balls), and the amount of powder in each vial (1.5 and 3 g).

The lack of a tight seal on the milling vials posed a significant problem, as during milling as much as 2/3 of the powder load was lost in some preliminary experiments. Likewise, unknown amounts of liquid nitrogen would enter the vials, changing the milling environment in poorly controllable ways. To alleviate this problem, the end caps were dipped in water before inserting into the ends of the vials. The water then filled the small gap between end cap and vial, and on freezing provided an effective seal. Material loss was reduced down to 0.3% over a 20-h milling period. Later experiments were all conducted using this procedure.

In runs without the water seal, to prevent condensation from ambient humidity the powder was recovered by simply opening the vial in a protective atmosphere. For experiments with the water seal, the vials were first placed in a vacuum chamber to sublimate the ice.

Product powders were characterized using various techniques. X-ray diffraction (XRD) measurements were conducted on a Philips X'pert MRD powder diffractometer using unfiltered Cu radiation ($\lambda = 1.5438$ Å), operating at 45 kV and 40 mA. XRD provided information about the phase composition of the prepared materials; in particular, identification of any products of partial thermite reaction occurring during the milling was of interest. Crystallite sizes were estimated from results of whole-pattern refinement of the XRD measurements using the GSAS [22,23] software package.

Particle size distributions (PSD) were measured by light scattering using a Beckman-Coulter LS230 Particle Counter.

To study the morphology of the prepared materials, powders were embedded in epoxy and cross-sectioned. After polishing, cross-sectioned samples were examined on a LEO 1530 Field Emission Scanning Electron Microscope (SEM) operated at 10 kV. For the 12Al·3CuO material, at least five representative SEM images of each sample were taken at a fixed magnification and processed to determine the average size distribution of CuO inclusions in the aluminum matrix.

Reactivity of the prepared materials was analyzed using differential scanning calorimetry (DSC) and a custom wire-ignition setup. DSC experiments were performed using a Netzsch Simultaneous Thermal Analyzer STA409PC. Samples were heated using different heating rates ranging from 2 to 20 K/min in argon. The custom wire-ignition apparatus is shown in Fig. 1. Its operation was presented in detail elsewhere [24] and it is only briefly described below. A slurry is prepared with the powder being tested placed in hexane or another quickly evaporating hydrocarbon liquid. A thin layer of the slurry is coated on a portion of a Nichrome® wire with a paintbrush and dried. The wire is then heated electrically with heating rates varying from 100 to 50,000 K/s. The wire temperature is monitored in real time using an infrared pyrometer. Simultaneously, the emission from the powder coating is measured with a photodiode, and the instant of powder ignition is detected by a spike in the photodiode signal. Thus, ignition temperatures at different heating rates are measured.

3. Results and discussion

The results are discussed in the context of comparing the properties of two nanocomposite materials with the same bulk composition of 12Al·3CuO. One of the materials was prepared using milling at the cryogenic temperature (assumed to be 77 K because the milling vials were submerged in liquid nitrogen) and the other was prepared using a planetary mill operated at room temperature. The same starting powders of Al and CuO were used to prepare both materials. In preliminary experiments it was observed that in the cryomill, the milling progress differs depending on the location of the milling vial. Specifically, the milling progress was faster and more consistent in the vials in the "top" position in the vial array. This effect is illustrated in Fig. 2. The black background in both images shown in Fig. 2 represents epoxy. In the embedded particles, CuO appears brighter than Al. Particles consisting primarily of either Al or CuO, with very few composite particles can be seen in the left image showing the powder retrieved from the vial in the lower position. Only composite particles including mixed Al and CuO are seen in the right image, showing the powder retrieved from the vial in the "top" position. Therefore, unless specifically stated otherwise, the following discussion will focus on results from "top" vials.

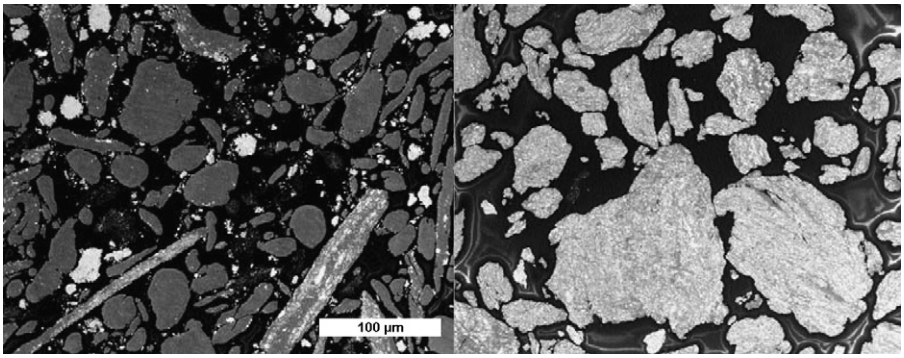

Fig. 2. Backscattered electron images of two 12Al·3CuO composites milled under nominally identical conditions. The powders are embedded in epoxy and cross-sectioned; images have the same magnification. The sample on the left was retrieved from a vial in the lower position, while the one on the right was retrieved from a vial in the "top" position. The powders were milled using a combination of 3 7/16 in. and 10 3/16 in. diameter steel balls.

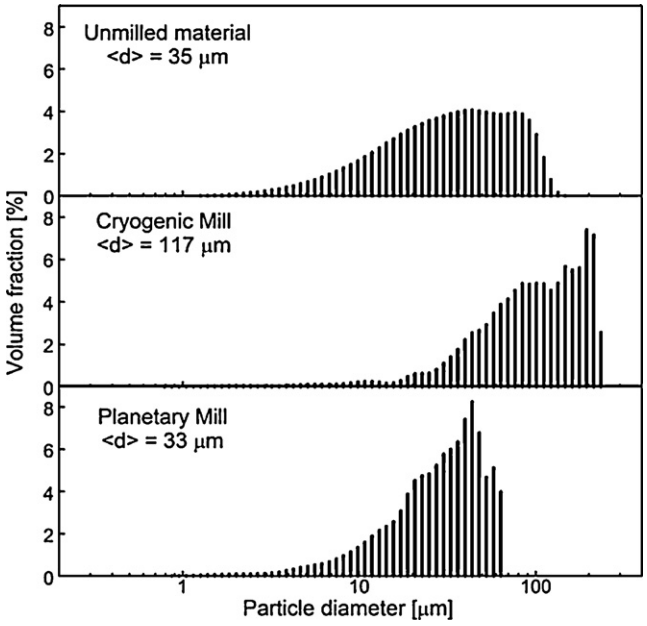

Fig. 3. Particle size distributions of unmilled 12Al·3CuO blend (starting material), and materials prepared by cryomilling and milling at room temperature in the planetary mill.

3.1. Material characterization

The size distributions for the starting powder blend used in both cryogenic and planetary mills, and for both produced composite powders are shown in Fig. 3. The particle size distribution for the powder prepared in the planetary mill was somewhat narrower than the initial size distribution of the powder blend. Alternatively, the composite powder prepared at the cryogenic temperature appeared to include quite a few relatively coarse particles. Note that the volume fractions of the particle size distributions shown in Fig. 3 were heavily affected by larger particles.

To compare the morphology of two prepared materials, the size distributions of CuO inclusions in Al matrix were measured using processing of the SEM images of the particle cross-sections. Representative SEM images are shown in Fig. 4. Images for the powders produced in both planetary and cryogenic mills showed brighter CuO inclusions within the darker Al matrix. The major apparent difference between the images was that the cryomilled material seems to be more homogeneous in terms of the distribution of CuO inclusions as compared to the material prepared in the planetary mill. The sizes of the CuO inclusions did not appear to be substantially different. This was confirmed by the size distributions shown in Fig. 5. These distributions were obtained by image processing.

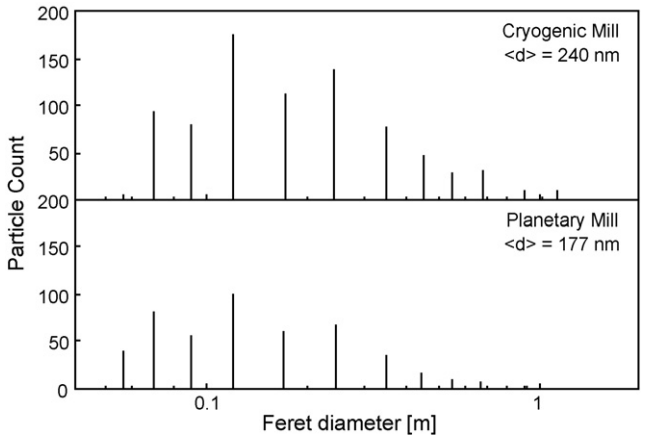

Fig. 5. Inclusion size distribution for 12Al·3CuO cryomilled and planetary milled materials.

The images were thresholded, lighter objects (CuO inclusions) were selected, and their Feret diameters were automatically determined using the UTHSCSA ImageTool package by S. Brent Dove available as freeware (http://ddsdx.uthscsa.edu/dig/itdesc.html). For both samples, the inclusions size distributions peaked at around 160 nm. The magnification used to collect the SEM images restricted the capability to resolve finer inclusions, so that the measurements are likely biased to larger inclusion sizes. This limitation is manifested by an apparent sharp drop off in the count number for inclusions under 80 nm. The difference in the mean inclusion size identified for the two powders in Fig. 5 was considered to be insignificant, and the inclusion size distributions are seen as effectively identical for both powders. Measured inclusion size distributions were used to estimate the polydispersity index defined as the ratio of the weighted volume average of the inclusion diameter over its number average diameter. The index values were 3.8 and 3.2 for the samples milled at room and cryogenic temperatures, respectively. This indicates a slightly narrower size distribution among inclusions produced by the milling at the cryogenic temperature.

Fig. 6 shows XRD patterns collected for the powders prepared in the cryogenic and planetary mills. The differences between the patterns were found to be subtle. The strongest peaks were, not unexpectedly, produced by the CuO and Al structures for both materials. However, the measured peak intensities were lower for the material prepared in the cryogenic mill. In addition, the peaks were wider for the material prepared at cryogenic temperatures, both indicators pointing out at a finer crystallite size for these materials as compared to their counterparts prepared in the planetary mill. A weak increase in the baseline indicating the presence of minor amounts of poorly crystalline aluminum oxides was occasionally observed for the powders prepared in the planetary mill.

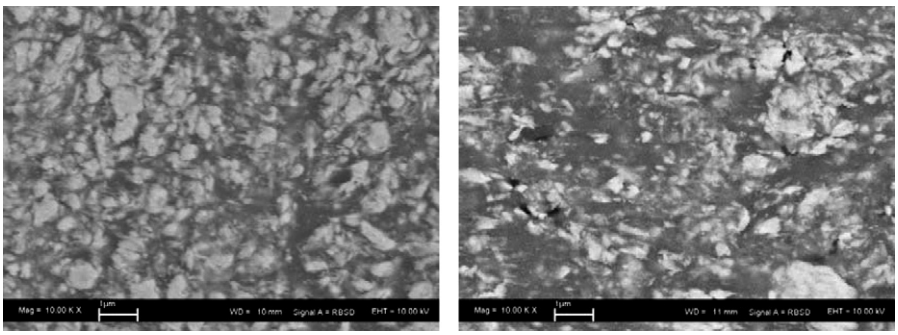

Fig. 4. Backscattered electron images of cross-sectioned 12Al·3CuO nanocomposite particles. The material on the left was cryomilled, and the material on the right was milled at room temperature in a conventional planetary mill. In both images, bright inclusions are CuO, while the dark matrix is Al.

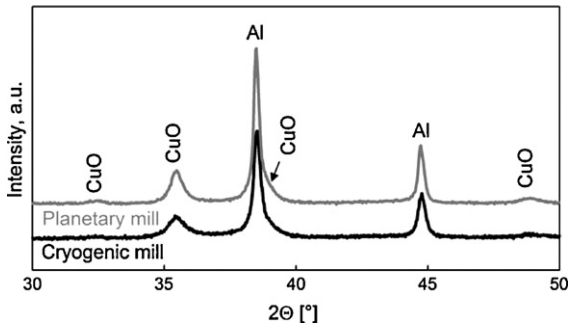

Fig. 6. XRD traces for both cryogenic and planetary mill. Both materials are very similar in composition with differences in the peak widths and intensity. This suggests that milling cryogenically will result in more refined components.

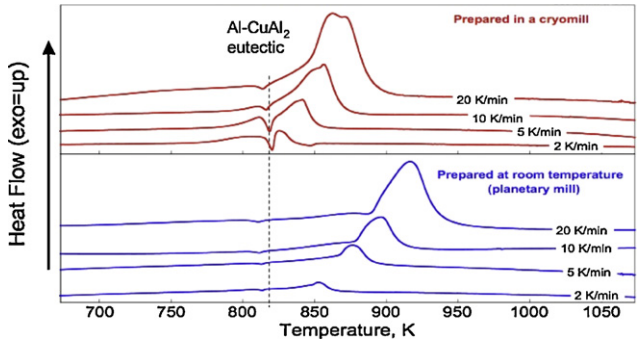

Fig. 8. Differential scanning calorimetry traces measured at various heating rates for materials prepared in cryogenic mill and planetary mill.

Such oxides could have formed as a result of undesirable thermite reaction occurring locally in the vial during the milling. Similar features were never detected for the powders prepared in the cryogenic mill.

Crystallite sizes were determined from the XRD patterns by whole-pattern refinement for all samples prepared in this study. Based on these results, it was attempted to compare milling runs with different milling parameters. For this purpose, a preliminary milling "progress function" Φ is suggested. As in Ref. [25] this progress function is based on the assumption that the refinement of the milled material is proportional to the work done by the milling tools. Therefore, the milling progress is roughly proportional to the number of collisions and the energy transfer per collision. The number of collisions is proportional to the operating frequency of the mill, f, and the milling time, t. The energy transferred from the milling tools to the powder in each collision is proportional to the mass of the milling tools, m_b, and inversely proportional to the powder load, m:

$$\Phi = m_b \cdot f \cdot \frac{t}{m}$$

Fig. 7 shows the Al and CuO crystallite size of the 12Al·3CuO composite powders as a function of Φ. The crystallite sizes for the unmilled component powders are shown for comparison, and the crystallite sizes achieved in the composite material prepared in the planetary mill are shown as horizontal dashed lines. Filled symbols represent results for vials in the top position, and open symbols represent bottom vials. As Fig. 7 shows, the crystallite size of both, Al and CuO, decreases with increasing milling progress function. The crystallite sizes achieved in the longest milling runs in the cryomill, corresponding to the greatest milling progress function, were smaller than in the material from the planetary mill.

In order to visualize the observed trend, Fig. 7B shows a curve that fit to all data points from vials in the "top" position. As can be seen, the milling progress function is suitable to compare different runs with different milling parameters. It is also evident that the progress in vials in the "bottom" position is less consistent.

Whole-pattern refinement was also used to estimate the overall Al/CuO ratio in the prepared materials to assess consistency between the samples and account for possible losses of individual components during preparation of composite materials. While for the targeted 12Al·3CuO composition, the mole ratio of Al/CuO is 4, the average mole ratio implied by the whole-pattern refinement was close to 4.5 and 4.8 for the materials prepared by room temperature and cryogenic milling, respectively. Given the uncertainties associated with the XRD pattern processing, the differences between the samples are considered to be insignificant.

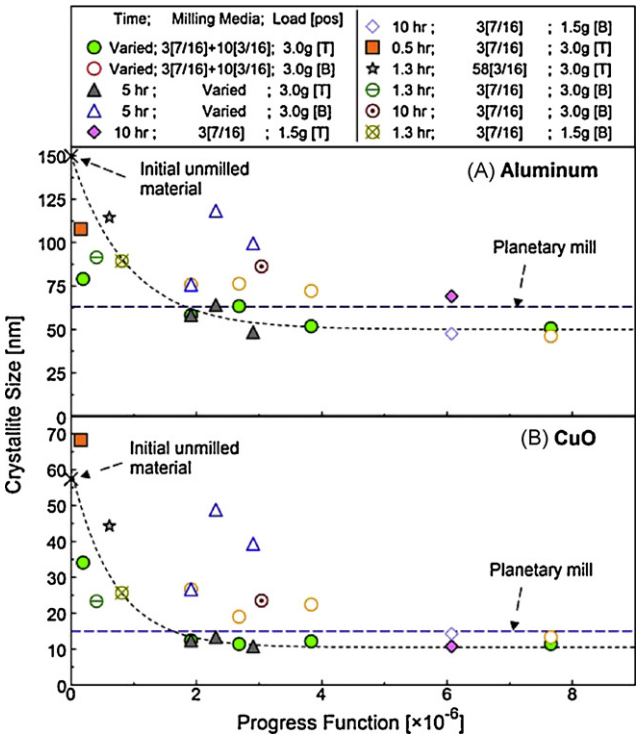

Fig. 7. Al (A) and CuO (B) crystallite sizes vs. the milling progress function. Both plots show the same experiments. [T] and [B] in the legend indicate top and bottom vial positions, respectively. Where indicated, the milling time was varied in the range 30–1200 min. Likewise, the mass, and number of the milling media were changed (various combinations of 7/16 in. and 3/16 in. steel balls).

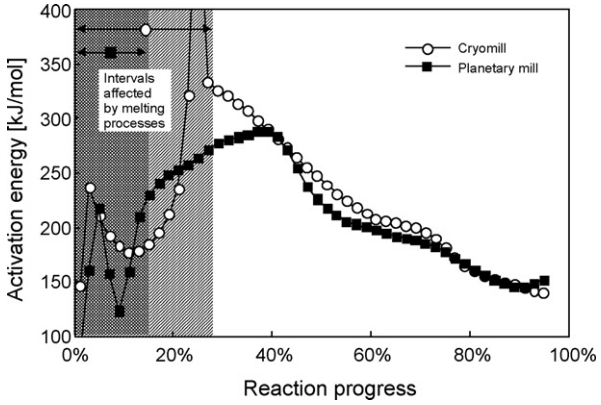

Fig. 9. Activation energy of the observed exothermic reaction as a function of the reaction progress calculated using results shown in Fig. 8 and an isoconversion processing algorithm proposed by Vyazovkin [27].

3.2. Material reactivity

DSC traces are shown in Fig. 8. Traces for both powders were measured at different heating rates in argon. It was observed that for both materials a relatively weak endothermic feature precedes the observed exothermic peak. The DSC traces were substantially different for the powders prepared at different milling temperatures. The endothermic peak was substantially stronger for the powder prepared at the cryogenic temperature. This peak occurred around 820 K and its position did not shift to higher temperatures at higher heating rates. Based on its parameters, this peak was assigned to a eutectic point between Al and the $CuAl_2$ alloy in the binary Al–Cu system [26]. In order for this transition to occur, the $CuAl_2$ alloy must have already been present, indicating that some of the copper was reduced and available to react with aluminum. Thus, the presence of a stronger endothermic feature corresponding to the eutectic reaction for the material prepared at the cryogenic temperature indicated its higher reactivity at temperatures lower than 820 K, compared to the material prepared in the planetary mill. Indeed a raised baseline observed clearly for the cryomilled material prior to the endothermic peak supports this reaction sequence. The higher reactivity at lower temperatures could be beneficial for achieving shorter ignition delays in practical applications for the materials prepared by cryomilling.

The second important difference in the DSC signals for the two materials has to do with position of the main exothermic peak clearly visible in all DCS traces. For the cryomilled material, this peak occurred at significantly lower temperatures as compared to the material prepared in the planetary mill.

In order to assess the kinetic relations for the reactions observed in the materials milled at cryogenic temperatures and at room temperature, the DSC results were processed by an isoconversion method. Specifically, the algorithm proposed by Vyazovkin [27] was implemented in MATLAB. The algorithm is used to process measurements at different heating rates simultaneously, resulting in an apparent activation energy that varies with the reaction progress. The result of this calculation is shown in Fig. 9. As can be seen in Fig. 8, the exothermic reactions are partially overlapped by melting reactions. This interferes with the unambiguous determination of individual reaction progress vs. temperature relations. Since this overlap is strongest at the lowest heating rate, the measurements at 2 K/min were omitted in this calculation. Still, the endothermic overlap is apparent in the E_A curves as irregularities around 10% reaction progress (planetary mill), and 25% (cryomill), respectively. Regardless of these difficulties, the curves show that at low reaction progress (<40%), the reaction in the cryomilled material is controlled by a process with a higher activation energy than the material milled at room temperature. At higher degrees of reaction, the differences between the materials are negligible.

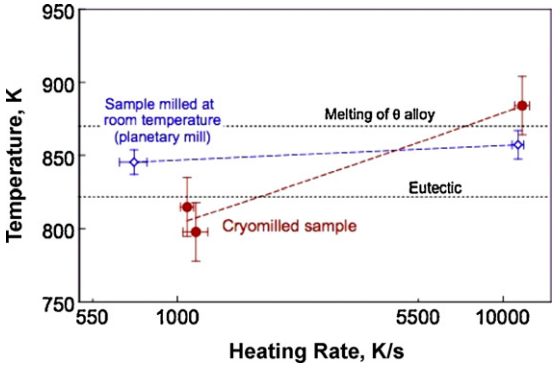

Fig. 10. Ignition temperatures measured as a function of the heating rate in the heated filament ignition experiments. The temperature of the Al–Al_2Cu eutectic, and the melting point of the θ–Al_2Cu alloy [26] are shown for reference.

The results of the heated filament ignition experiments are shown in Fig. 10. Both materials were heated at different heating rates. In both cases, the measured ignition temperatures were close to the temperature range in which the eutectic melting of Al and $CuAl_2$ alloy occurs in the binary Al–Cu system [26]. However, the observed effect of the heating rate on the ignition temperature was greater for the material prepared at cryogenic temperature. It can be initially proposed that the ignition in the material prepared in the planetary mill is controlled by the eutectic melting in the sample, while for the material prepared in the cryomill the reaction may be thermally activated and may initiate even before the eutectic melting.

4. Conclusions

The feasibility of preparing reactive nanocomposite materials by ARM performed at cryogenic temperatures was established. The inclusions of the harder phase (metal oxide) distributed in the matrix of a softer component (aluminum) were approximately of the same size for materials prepared at both cryogenic and room temperatures. However, the inclusions were distributed more uniformly for the materials prepared in the cryomill. X-ray diffraction analysis showed that the crystallite sizes of the components mixed by ARM performed at the cryogenic temperature were finer compared to their counterparts produced by the room temperature milling. It was also observed that effectively no reacted material can be detected in the nanocomposite prepared at cryogenic temperature. Thermal analysis indicated that the material prepared at cryogenic temperatures was more reactive at low temperatures. It was also observed that the reaction mechanisms and activation energies differ for the materials with the same bulk chemical composition prepared at different temperatures.

Acknowledgements

This work was supported in parts by Defense Threat Reduction Agency and by RDECOM-ARDEC, Picatinny. Additional support for this research by The Emil Buehler Perpetual Trust is appreciated.

References

[1] E.L. Dreizin, Prog. Energy Combust. Sci. 35 (2009) 141–167.
[2] J.A. Puszynski, C.J. Bulian, J.J. Swiatkiewicz, Mater. Res. Soc. Symp. Proc. 896 (2006) 147–158.
[3] T.M. Tillotson, A.E. Gash, R.L. Simpson, L.W. Hrubesh, J.H. Satcher Jr., J.F. Poco, J. Non-Cryst. Solids 285 (2001) 338–345.
[4] W.C. Danen, B.S. Jorgensen, J.R. Busse, M.J. Ferris, B.L. Smith, Proceedings of the 221st ACS National Meeting, San Diego, CA, United States, 2001 (Abstracts of Papers).
[5] W.L. Perry, B.C. Tappan, B.L. Reardon, V.E. Sanders, S.F. Son, J. Appl. Phys. 10 (2007), 064313/1–064313/5.
[6] A. Prakash, A.V. McCormick, M.R. Zachariah, Adv. Mater. 17 (2005) 900–903.
[7] K.C. Walter, D.R. Pesiri, D.E. Wilson, J. Propul. Power 23 (2007) 645–650.
[8] M.L. Pantoya, J.J. Granier, Propell. Explos. Pyrotech. 30 (2005) 53–62.
[9] E.L. Dreizin, M. Schoenitz, US Patent 7,524,355 B2 April 28 (2009).
[10] M. Schoenitz, T.S. Ward, E.L. Dreizin, Proc. Combust. Inst. 30 (2005) 2071–2078.
[11] S. Umbrajkar, M.A. Trunov, M. Schoenitz, E.L. Dreizin, R. Broad, Propell. Explos. Pyrotech. 32 (2007) 32–41.
[12] E.L. Dreizin, M. Schoenitz, Y.L. Shoshin, M.A. Trunov, Int. Annual Conf. of ICT, 36th (Energetic Materials) (2005) 138/1–1138/.
[13] S.M. Umbrajkar, M. Schoenitz, E.L. Dreizin, Propell. Explos. Pyrotech. 31 (2006) 382–389.
[14] S.M. Umbrajkar, S. Seshadri, M. Schoenitz, V.K. Hoffmann, E.L. Dreizin, J. Propul. Power 24 (2008) 192–198.
[15] S.M. Umbrajkar, M. Schoenitz, S.R. Jones, E.L. Dreizin, J. Alloys Compd. 40 (2005) 70–77.
[16] R.J. Perez, B. Huang, E.J. Lavernia, Nanostruct. Mater. 7 (1996) 565–572.
[17] D.B. Witkin, E.J. Lavernia, Prog. Mater. Sci. 51 (2006) 1–60.
[18] A.V. Borissova, S. Deledda, B.C. Hauback, J. Alloys Compd. 481 (2009) L24–L26.
[19] W. Xiong, P. Li, D. Xie, X. Zheng, C. Zeng, X. Qu, Xiyou Jinshu Cailiao Yu Gongcheng/Rare Metal Mater. Eng. 38 (2009) 365–367.

[20] D.M. King, Y. Zhou, L.F. Hakim, X. Liang, P. Li, A.W. Weimer, Ind. Eng. Chem. Res. 48 (2009) 352–360.
[21] J.-H. Lee, S.J. Hwang, Rev. Adv. Mater. Sci. 18 (2008) 289–292.
[22] T.S. Ward, M.A. Trunov, M. Schoenitz, E.L. Dreizin, Int. J. Heat Mass Trans. 49 (2006) 4943–4954.
[23] A.C. Larson, R.B. Von Dreele, Los Alamos National Laboratory Report LAUR 86-748, 2000.
[24] B.H. Toby, J. Appl. Cryst. 34 (2001) 210–213.
[25] T.S. Ward, W. Chen, M. Schoenitz, R.N. Dave, E.L. Dreizin, Acta Mater. 53 (2005) 2909–2918.
[26] T.B. Massalski, J. Phase Equilibr. 1 (1980) 27–33.
[27] S. Vyazovkin, J. Comput. Chem. 22 (2001) 178–183.